High Purity Germanium Detector Calibration at ISOLDE

Guðmundur Kári Stefánsson Summer Student of Maria Borge

September 5, 2013

Abstract: *This Summer Student Project involved the test and calibration of two High Purity Coaxial Germanium gamma-ray detectors; Canberra models GC7020 (old, from 1990), and GX6020 (new, from July 2013), used at the ISOLDE experimental Hall at CERN. In this report I present and discuss the calibration and efficiency curves obtained for both detectors, and the methods used to obtain them.*

1 Introduction

Germanium detectors are essential instruments in high-resolution γ-ray spectroscopy applications. Different variations of Ge detectors are available from commercial manufacturers, which have different performance characteristics. The detectors I worked with are referred to as a Coaxial Ge detectors, High Purity Germanium (HPGe) detectors, or intrinsic Ge detectors.

Germanium detectors are semiconductor diodes having a P-I-N structure in which the Intrinsic (I) region is sensitive to ionizing radiation, particularly X rays and gamma rays. Under reverse bias, an electric field extends across the intrinsic or depleted region. When photons interact with the material within the depleted volume of a detector, charge carriers (holes and electrons) are produced and are swept by the electric field to the P and N electrodes. This charge, which is in proportion to the energy deposited in the detector by the incoming photon, is converted into a voltage pulse by an integral charge-sensitive preamplifier.

Because germanium has a relatively low band gap, these detectors must be cooled in order to reduce the thermal generation of charge carriers to an acceptable level. Otherwise, leakage current induced noise would destroy the energy resolution of the detector. Therefore, the detector is normally mounted in a vacuum chamber which is attached to a liquid nitrogen Dewar.

In order to reduce attenuation of gamma rays before they interact with the detector, a thin end window is made at the entrance face of the detector. This window increases the transmission of lower energy gammas compared to normal aluminium housing [1]. On the other hand however, to reduce background noise, the detector can be surrounded by a thick shielding material, usually materials with a high atomic number, such as lead.

1.1 Signal Electronics

Figure 1 illustrates a simple counting system with an HPGe detector, including a high voltage power supply, a preamplifier, a main amplifier, an Analog-to-digital converter (ADC), and multichannel analyzer (MCA).

The charge sensitive preamplifier senses the charge collected on the capacitor if a γ-ray interaction occurs in the biased intrinsic region of the detector, and outputs a voltage signal where the amplitude is proportional to the energy deposited in the γ-ray interaction. The charge accumulated on the capacitor must be removed, giving the preamp signal an exponential decay tail (see C in figure 1). The preamplifier signal is then integrated, and shaped by the main amplifier, giving it an optimum signal-to-noise ratio, and is subsequently sent for digitization in an analog-to-digital converter (ADC) which is usually the heart of a multichannel analyzer (MCA). The MCA then bins similar amplitudes together and stores them in a multichannel memory, which can subsequently be used to give a pulse height histogram [2].

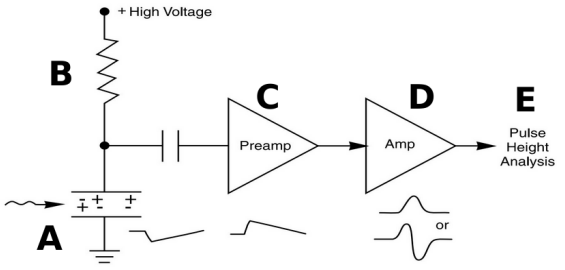

Figure 1: A simple counting system, including: A) a HPGe detector; B) a high voltage power supply; C) a charge sensitive preamp; D) a main amplifier; E) pulse height analysis modules (usually a multichannel analyzer (MCA) with an analog-to-digital converter (ADC).

1.2 Energy Calibration

In gamma-ray spectroscopy with germanium detectors, the pulse height scale must be calibrated in terms of absolute gamma-ray energy. To calibrate any gamma spectrum it is necessary to properly identify the centroid of some known energy peaks, and then a calibration curve can be determined to scale from channels to energy units.

1.3 Efficiency

Any measurement of absolute emission rates of gamma rays requires knowledge of the detector efficiency. The emission rate for a point source can then be calculated measuring the full-energy peak area over a fixed time and by determining the detector solid angle from its dimensions and the source-detector spacing [2]. Although efficiencies of germanium detectors can be estimated from published measurements or calculations for detectors of similar size, and as long-term change in charge collection efficiency and/or window thickness can lead to drifts in the detector efficiency, the accuracy of results based on such values will not be much better than $10 - 20\%$ [1]. Therefore, users of such de-

tectors will normally carry out their own periodic efficiency calibrations of their germanium detectors using sources calibrated by some other means.
The relative efficiency of a Ge detector, $\varepsilon_{\text{rel}}(E_\gamma)$, of a given peak with energy E_γ, is defined as

$$\varepsilon_{\text{rel}} = \frac{N_\gamma}{t_\gamma P A_0 e^{-\lambda \Delta t}} \tag{1}$$

where N_γ is the total number of registered counts in the peak, t_γ is the *life-time* of the measurement, P is the branching ratio of the given peak with energy E_γ, and A_0 is the activity, and λ is the decay constant of the isotope sample and Δt is the time period between the activity date and measurement date.
The relative efficiency, ε_{rel} can be corrected for geometric effects, by calculating the effect of the solid angle ε_Ω, giving the detector *intrinsic efficiency*:

$$\varepsilon_{\text{int}} = \frac{\varepsilon_{\text{rel}}}{\varepsilon_\Omega} \tag{2}$$

Once the efficiency of a detector has been measured at several energies using calibrated sources, it is useful to fit a curve to these points in order to describe the efficiency over a given energy range. Several empirical formulas to estimate the efficiency of HPGe detectors have been described in the literature. In [1] it is suggested that $\ln(\varepsilon)$ may be related to a polynomial of $\ln E$:

$$\ln(\varepsilon) = \sum_{i=1}^{N} a_i (\ln E)^{i-1} \tag{3}$$

where low N tend to give good results for a low number of data points over a wide energy range. I refer to this function as the *Log-Poly*-type. Furthermore, the following function,

$$\ln(\varepsilon) = \sum_{i=1}^{4} a_i (\ln E)^{i-1} + a_4/E^3 \tag{4}$$

was also mentioned in my discussions with Jan Kurcewicz and my supervisor, Maria, - I refer to this function as the *Poly*-type. Other fitting functions, such as those by Jäckel et al. [3], and Gallagher et al. [4], have been proposed, but were not considered in this work.

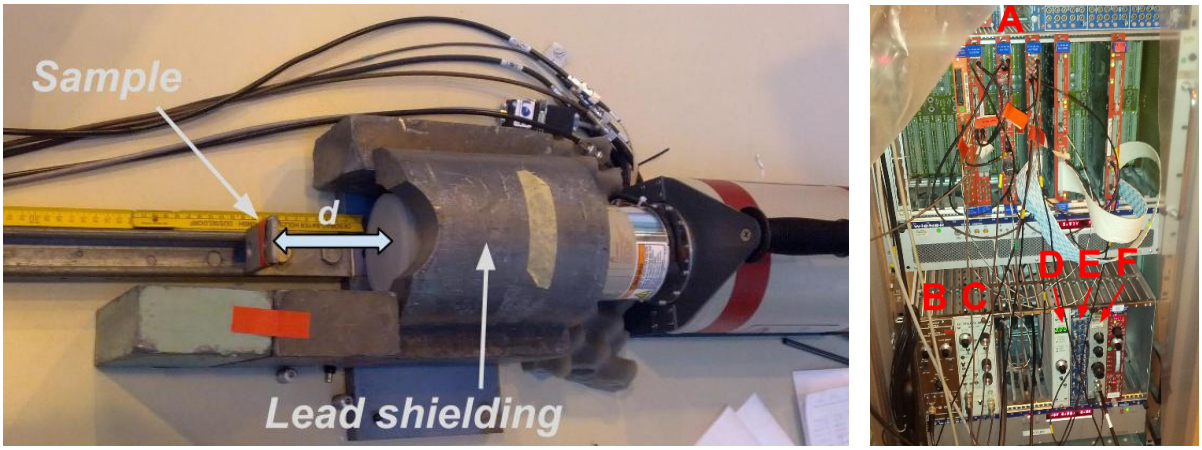

(a) **(b)**

Figure 2: a) A picture showing the experimental setup. The sample was placed on a metal slide at a distance d, measured with a ruler, perpendicular from the detector end-cap (removed during spectra measurements). Furthermore, the picture shows the lead shielding which helped in shielding the detector from background radiation.; b) A picture of the NIM modules used (with the newer detector): A) ADC B) Pulse generator (E-300), C) AFT research amplifier (model 2025), E) HV Power supply (model 3106 D), F) Discriminator (model 620AL), G) Timing Filter (Ortec model 454)

2 Experimental methods

A schematic diagram of the experimental setup can be seen in figure 2, defining the distance d from the detector end-cap to the sample, along with illustrating the lead shielding that was used to reduce background noise.
The calibration process was as follows:

- A given isotope sample was placed at a distance d measured perpendicular from the detector end-cap. For the newer detector, the end-cap was then carefully removed.
- A spectrum was accumulated, with a measurement time of t_{spectrum}, which was corrected for background; the same background spectra (adjusted to the measurement time of the spectra) being used for all subsequent spectra.
- The resulting corrected spectra was analysed: A Gaussian was fitted using `rootpy` (most often with an additional manual subtraction to correct better for the background) for each of the peaks listed in table 2 for that isotope, recording the center and FWHM of the peak.
- Ultimately the *real energy* of each peak was

plotted as a function of *observed channel position*, producing the characteristical linear calibration curve of the detector.

Before performing systematic measurements with each detector, preliminary tests were performed, which constisted of adjusting the shaping time of the amplifier signal, logic gate time, and performing pole zero adjustments. All measurements for the GX6020 detector were performed with a shaping time of 6 μs, and an amplifier course gain of 20 and fine gain of 7.09, while a shorter shaping time of 3 μs and an amplifier course gain of 5, and fine gain of 7.50 was used for the GC7020 (old) model.

Three different computers were used in the ISOLDE Experimental Hall: a single board VME computer called `caisol`, which did the actual data acquisition (DAQ), and an analysis computer, called `pcepisdaq3` which could save the data acquired from `caisol`, along with a third computer, `pcepisdaq6`, that could interface with the other two computers via `ssh`. All of the analysis was done with the `Python` programming language, along with `pyroot`, a pythonistic version of `ROOT` - a data analysis language commonly used at CERN - and `Go4`, a graphical interface to `ROOT`, found on `pcepisdaq3`.

Figure 3 illustrates the detector geometry, along with the parameters used in the intrinsic efficiency calculations. The distances d_1 and d_2 are measured from the detector end-cap. The end-cap was removed during spectra measurements with the newer detector, as it was easily removable.

For the calibration, four sources were used in total; ^{60}Co , ^{137}Cs , ^{133}Ba and ^{152}Eu . Table 2 shows the emission lines of each of these sources, along with their activity, and reference number.

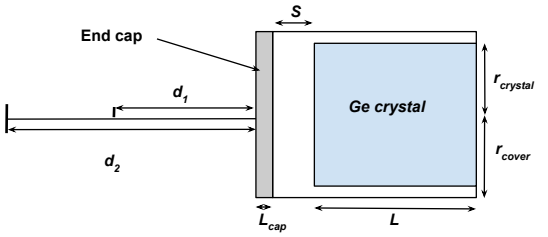

Figure 3: A schematic diagram of the detectors under study, defining the dimensions used in the analysis: the two measurement distances, from the sample to end cap; $d_1 = 12.2$ cm, and $d_2 = 20.0$ cm. The length of the crystal L, and the window-to-crystal distance S can be found in table 1. In the analysis for the newer detector model it was assumed that the crystal completely covered the whole detector shell, giving a diameter of $2r_{\text{crystal}} = 2r_{\text{shell}} = 69$ mm.

Detector:	***Older***	***Newer***
Model number:	GC7020	GX6020
Manufacturer:	Canberra	Canberra
Date of first usage:	1990	July 2013
Bias Voltage:	+4000 V	+4500 V
Resolution at 122 keV**:**	1.05 keV	0.92 keV
Resolution at 1.33 MeV**:**	2.0 keV	1.85 keV
Window material:	*Aluminum*	*Carbon*
Crystal volume (of NaI):	70%	60%
Endcap diameter:	89 mm	69 mm
Crystal diameter, $2r_{\text{crystal}}$***:***	74 mm	69 mm (*)
Window-crystal dist, S:	6 mm	5 mm (*)
Crystal length, L:	63 mm	70 mm (*)

Table 1: Comparison of the two detectors used. I frequently refer to the GC7020 model as the older detector, and the GX6020 model as the newer detector. The values marked by an asterisk (*) are not the exact values specifically measured for the new detector, but were assumed as they are listed as common values for this detector-type (see Canberra [5]). The corresponding values for the older detector were specifically determined by Canberra for this exact detector (values acquired by email inquiry).

^{60}Co	**Activity [Bq]**:	40000
	Reference No.	3986RP
	1173.238(4)	99.89(2)
	1332.502(5)	99.983(1)
^{137}Cs	**Activity [Bq]**:	22420
	Reference No.	2668RP
	661.660(3)	85.20(2)
^{133}Ba	**Activity [Bq]**:	30000
	Reference No.	4205RP
(*)	53.1610(15)	2.20(4)
(*)	79.6127(15)	2.63(8)
	80.9975(10)	34.1(5)
	276.4000(15)	7.17(4)
	302.8527(10)	18.32(7)
	356.0146(15)	62.0(3)
	383.8505(15)	8.93(6)
^{152}Eu	**Activity [Bq]**:	30000
	Reference No.	4206RP
	121.7824(4)	28.30(15)
	244.6989(10)	7.54(5)
	344.2811(19)	26.52(18)
	411.126(3)	2.246(16)
	443.965(4)	3.10(2)
	778.920(4)	12.94(7)
	867.390(6)	4.23(3)
	964.055(4)	14.60(8)
	1085.842(4)	10.09(4)
(*)	1089.767(14)	1.737(8)
	1112.087(6)	13.56(6)
	1212.970(13)	1.423(10)
	1299.152(9)	1.630(10)
	1408.022(4)	20.80(12)

Table 2: Sources used, showing their ISOLDE reference numbers, along with emission line data from Debertin et al. [6]. All energies are in keV. The activity was dated at March 2007 - I assumed 1st of March in my analysis. The lines marked with (*) were not considered in the analysis.

3 Results and discussion

Below I compare the calibration and resolution curves obtained for both detectors. Finally, the results from the efficiency measurements for both detectors are presented.

3.1 Calibration and Resolution

Figure 4 compares the calibration curves for both detector models. Both are highly linear in the energy range studied, and fitting a line using a least-square method gave the parameters shown in table 3.

	Slope [keV/channel]	Offset [keV]
GC7020	0.618636(1)	−54.8417(5)
GX6020	0.371519(1)	−31.44116(51)

Table 3: Slopes and offsets for the calibration curves shown in 4a for GC7020 and 4b for detector GX6020, obtained by the least-squares method.

Figure 5a) and b) shows how the resolution changes as a function of energy for both detectors - it increases linearly with increasing energy. Table 4 compares the measured and certified resolution values at the two emission lines shown in table 1.

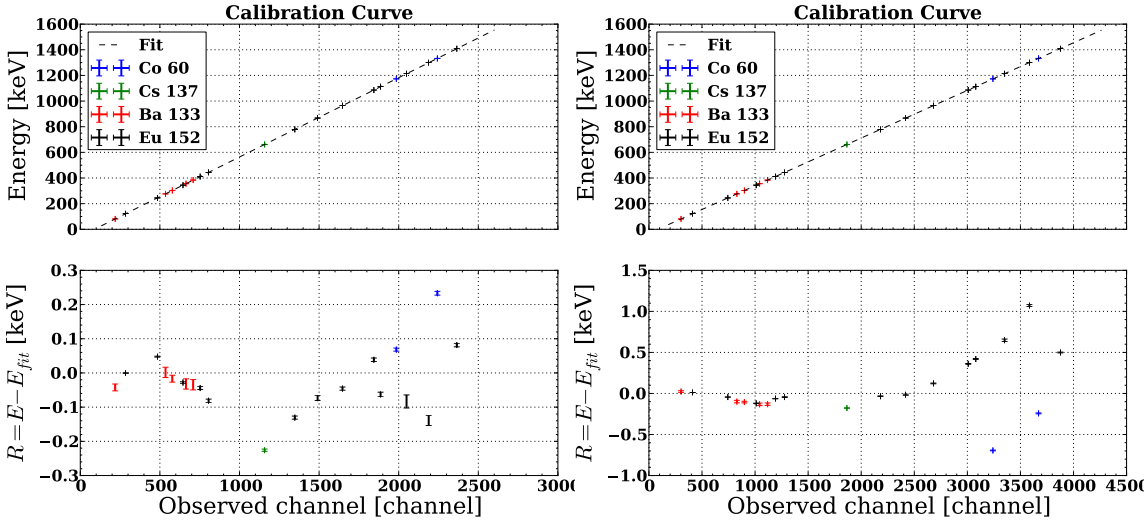

(a) GC7020 model (older)

(b) GX6020 model (newer)

Figure 4: Calibration curves for (a) the GC7020 (older) model, and (b) the GX6020 model along with showing the corresponding residuals - the *real energy of the peak* minus the fitted value. Both models exhibit a high linear behaviour in the energy range studied, the GC7020 model, however, shows less deviations that are more randomly dispersed from the fitted curve (see residuals), implying a better calibration.

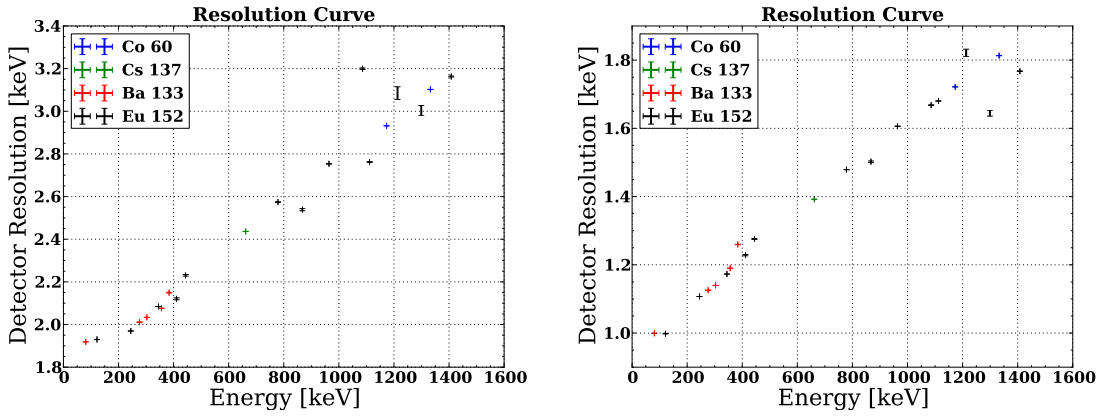

(a) GC7020 model (older)

(b) GX6020 model (newer)

Figure 5: Resolution curves for both detector models. We immediately see that the resolution of the GX6020 (newer) model is much better than the resolution of the GC7020 model (older). As expected, the resolution linearly increases with increasing energy, for both models. Comparing the plot on the left with the manufacturer resolution values found in 1, we clearly see that the resolution of the old detector has degraded. The measured resolution for the newer detector, however, is close to the certified values by the manufacturer.

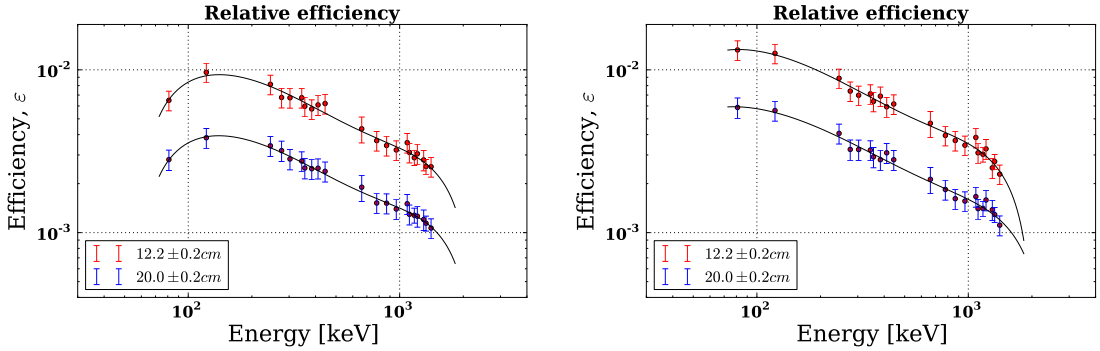

(a) GC7020 model (older)

(b) GX6020 model (newer)

Figure 6: Comparison of the relative, ε_{rel} efficiencies for both detector models. Noting that the scales are the same on both plots, we easily see that the relative efficiency of the newer detector is better for both distances. The fitted curves are of the *Poly-Log* type (see Eq. 3).

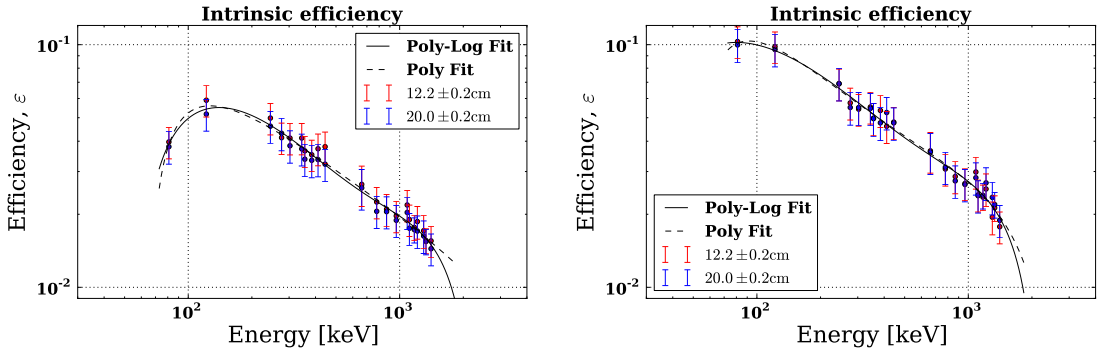

(a) GC7020 model (older)

(b) GX6020 model (newer)

Figure 7: Comparison of the intrinsic, ε_{int} efficiency data for both detector models, calculated for both distances, along with fitted curves (*Poly-Log* and *Poly* fits). We see that the intrinsic efficiency of the newer detector is better for both distances.

3.2 Efficiency

Figure 6 shows the measured relative efficiency for both detector models, for two distances, $d_1 = 12.2$ cm and $d_2 = 20.0$cm along with a least-squares fitted curve of the Poly-Log type (Eq. 3).

Figure 7 shows the intrinsic efficiency of both detectors, calculated from the solid angle; $\varepsilon_\Omega = 2\pi(1 - \cos(\theta))$ where θ is half the apex angle of a cone with its base at the detector window, and apex at the radioactive source. Also shown are two differently fitted curves - the `Poly-Fit`-type as seen in eq. 3 and the Poly-type, as seen in eq. 4. Both data points fall really closely together, so for the least-square fitting, both datasets (from 12.2 cm, and 20.0 cm) were used.

From the χ^2 values for the *Poly-log* fits for 12.2 cm and 20.0 cm data, we see evidence of very good fits. However, noting that the a_4 parameter is 5 or 6 orders of magnitude larger from the other parameters for the *Poly*-fit, we could say that the *Poly-Log* fit seems to be more confined with respect to best-fit parameter values.

Energy	122 keV (^{133}Ba)	1.33 MeV (^{60}Co)
Certified (GC7020):	1.05 keV	2.00 keV
Measured (GC7020):	1.93 keV	3.10 keV
Certified (GX6020):	0.92 keV	1.85 keV
Measured (GX6020):	0.99 keV	1.81 keV

Table 4: Comparison of measured and certified resolution values by the manufacturer at two energy values near the extreme of the detector operating range, for both detector models.

Model: **GC7020**

Fit	12.2 cm	20.0 cm	Poly-Log	Poly
a_0	−1.12	−0.47	−6.59	0.57
a_1	0.75	0.31	4.39	−0.19
a_2	−0.18	−0.08	−1.07	0.02
a_3	0.02	0.01	0.12	−0.00
a_4	−0.00	−0.00	−0.00	−26112.91
χ^2	$2.08 \cdot 10^{-6}$	$1.29 \cdot 10^{-7}$	0.01405	0.01407

Table 5: Fitting results along with the calculated χ^2 value for each fit, for the GC7020 model. Fits are shown in figures 6a and 7a.

Model: **GX6020**

Fit	12.2 cm	20.0 cm	Poly-Log	Poly
a_0	−0.70	−0.24	−4.80	1.86
a_1	0.51	0.17	3.47	−0.77
a_2	−0.13	−0.04	−0.90	0.11
a_3	0.01	0.00	0.10	−0.01
a_4	−0.00	−0.00	−0.00	−26516.02
χ^2	$1.90 \cdot 10^{-6}$	$4.89 \cdot 10^{-7}$	0.03814	0.03825

Table 6: Fitting results along with the calculated χ^2 value for each fit, for the GX6020 model. Fits are shown in figures 6a and 7a.

4 Conclusion

In short, my project has been about the testing and simulation of High Purity Germanium γ-ray detectors at ISOLDE.

Both detectors were calibrated successfully, obtaining their characteristic calibration curve, where both detectors exhibited a high degree of linearity. Furthermore, we see that the resolution for the older model GC7020 has degraded by a substantial amount, while the newer model GX6020 has resolution values similar to the ones reported by the manufacturer. This could most likely be attributed to the older model being used as a beam dump in the MINIBALL experiment, exposing it to a lot of neutron radiation, which is known to have detrimental effects to Ge crystals.

From the resolution curves obtained we see that even though the older detector has a larger active volume than the newer detector (70% of NaI vs 60% of NaI), it has a substantially lower relative, and intrinsic efficiency. From figures 6 and 7 we can readily see the effect of the different detector windows being used; the γ-ray attenuation is much higher for the older detector, showing a dip in the efficiency curves, both for ε_{rel} and ε_{int}.

After this summer I have gotten experience in working in an international scientific environment; in communicating and discussing scientific results in both oral and written English, as a part of the ISOLDE research group at CERN. The work done during this summer involved a lot of experimental work at the ISOLDE experimental hall, giving me experience in working independently at a nuclear research lab. On the hardware side I have become familiar with various NIM modules commonly found in an analog nuclear counting system. On the software side, I have become familiar with *rootpy*, a python version of ROOT, the most commonly used data-analysis program at CERN, which I did not know before. Overall, I am very content with my research project, giving me a valuable experience which will undoubtedly come to good use later in my scientific career.

Acknowledgments

I want to thank my supervisor, Maria Borge, for all her help and support during this project. I also want to thank Olof Tengblad for his help (tackar!) and Jan Kurcewicz for answering my endless questions about everything related to these detectors. Moreover, I want to thank the ISOLDE group, for having me here, and giving me a glimpse of how real science works, and lastly of course the Summer Student Program at CERN, which has enabled me to experience a great summer here in Switzerland and neighbouring countries.

5 References

[1] Esteban Picado Sandi. *Advances in Gamma-Ray Detection with Modern Scintillators and Applications*. PhD thesis, Universidad Complutense de Madrid, 2013.

[2] W. R. Leo. *Techniques for Nuclear and Particle Physics Experiments*. Springer-Verlag, 1994.

[3] B. Jäckel, W. Westmeier, and P. Patzelt. On the photopeak efficiency of germanium gamma-ray detectors. *Nuclear Instruments and Methods in Physics Research Section A: Accelerators, Spectrometers, Detectors and Associated Equipment*, 261(3):543 – 548, 1987.

[4] William J. Gallagher and Sam J. Cipolla. A model-based efficiency calibration of a si(li) detector in the energy region from 3 to 140 kev. *Nuclear Instruments and Methods*, 122(0):405 – 414, 1974.

[5] Canberra. *Germanium Detectors User's manual*, 2011.

[6] K. Debertin and R. G. Helmer. *Gamma-and X-ray Spectrometry with Semiconductor Detectors*. Elsevier Science Publishers B.V., 1988.